

The fraction of condensed counterions around a charged rod: Comparison of Poisson-Boltzmann theory and computer simulations

Markus Deserno¹, Christian Holm¹ and Sylvio May²

¹ *Max-Planck-Institut für Polymerforschung, Ackermannweg 10, 55128 Mainz, Germany*

² *Institut für Biochemie und Biophysik, Friedrich-Schiller-Universität Jena, Philosophenweg 12, 07743 Jena, Germany*
(February 5, 2020)

We investigate the phenomenon of counterion condensation in a solution of highly charged rigid polyelectrolytes within the cell model. A method is proposed which – based on the charge distribution function – identifies both the fraction of condensed ions and the radial extension of the condensed layer. Within salt free Poisson-Boltzmann (PB) theory it reproduces the well known fraction $1 - 1/\xi$ of condensed ions for a Manning parameter $\xi > 1$. Furthermore, it predicts a weak salt dependence of this fraction and a break down of the concept of counterion condensation in the high salt limit. We complement our theoretical investigations with molecular dynamics simulations of a cell-like model, which constantly yield a stronger condensation than predicted by PB theory. While the agreement between theory and simulation is excellent in the monovalent, weakly charged case, it deteriorates with increasing electrostatic interaction strength and, in particular, increasing valence. For instance, at a high concentration of divalent salt and large ξ our computer simulations predict charge oscillations, which mean-field theory is unable to reproduce.

I. INTRODUCTION

Strongly charged linear polyelectrolytes use their counterions to reduce their line charge density¹. This phenomenon has led to the concept of *counterion condensation*^{2,3}, and although it has been introduced a long time ago, up to date various viewpoints about this subject exist in the literature^{1,4}. Here we will investigate its appearance within the commonly used *cell model*^{5,6}: an infinitely long charged rod enclosed in a cylindrical cell together with its counterions — with and without added salt.

In the salt free case this model can be solved analytically within nonlinear Poisson-Boltzmann (PB) theory^{7,8}, which thus affords a particularly clear view on Manning-Oosawa counterion condensation, as has been demonstrated by Zimm and Le Bret^{9,10}. Going beyond salt free PB theory questions arise: How closely condensed and tightly bound is the “condensed layer”? What distinguishes condensed from uncondensed counterions? When is the *mean-field* level PB theory a good approximation for real systems? And how does the presence of salt affect the condensation phenomena?

Recently Manning proposed the idea that there exists a clear distinction between (i) a condensed layer and (ii) a distant, more diffuse “Debye-Hückel” cloud¹¹. In the integrated radial counterion distribution function this is supposed to be detectable as an inflection point, which separates the two regions. Here we argue that this is not quite in accord with PB theory without added salt: There is an inflection point in the distribution function, but it is not related to the condensation phenomenon. If however the distribution function is plotted against *logarithmic* radial distance, an inflection point appears which exactly divides the counterions into condensed and uncondensed ones, as previously pointed out by Belloni¹². Since this feature has largely gone unnoticed in the study

of polyelectrolytes, we found it worthwhile to present its derivation within PB theory in a short and explicit form and also to point out its *practical* usability. To this end, we present computer simulations, compare them to PB theory, and demonstrate that this criterion can indeed be extended to quantify counterion condensation even beyond the scope of PB theory.

In the case of added salt no analytical solution of the PB equation is known, so any potential inflection point criterion is more difficult to analyze. Still, the PB equation can be solved numerically, suggesting that the presence of monovalent salt decreases the *extension* of the condensed layer, but leaves the *amount* of condensed counterions largely unaffected. We show that this behavior is well reproduced in computer simulations for monovalent salt. We also present a simple criterion for deciding, from which salt concentration on the concept of Manning condensation is no longer meaningful. In the regime of strong electrostatics, high valence and much added salt the PB predictions deviate qualitatively from simulation results. In particular, the simulation shows a pronounced overcharging, which is absent on the *mean-field* PB level.

This paper is structured as follows: In Secs. II and III we recapitulate the main ingredients of the PB solution for the salt free cell model and illustrate the connection of Manning condensation with the inflection point criterion mentioned above. This is followed – in Sec. IV – by a comparison of the salt free PB results with computer simulations. In Secs. V and VI we discuss the concept of counterion condensation in the presence of salt and to this end derive a PB equation for the ensemble of constant salt molecules. Its results are compared with simulations in Sec. VII. Details of our simulation method can be found in the Appendix.

II. PB-THEORY FOR A CHARGED ROD WITHOUT ADDED SALT

Consider an infinitely long cylinder of radius r_0 and line charge density $\lambda > 0$, which is coaxially enclosed in a cylindrical cell of radius R . Global charge neutrality of the system is ensured by adding an appropriate amount of oppositely charged (monovalent) counterions.

Within PB theory these counterions are replaced by a cylindrically symmetric counterion *density* $n(r)$ (r is the radial coordinate) which gives rise to an electrostatic potential $\Phi(r)$ satisfying the Poisson equation

$$\left(\frac{d^2}{dr^2} + \frac{1}{r} \frac{d}{dr} \right) \Phi(r) = \frac{e}{\epsilon} n(r) \quad (1)$$

with ϵ being the dielectric constant outside the cylinder¹³ and e the (positive) unit of charge. Conversely, this potential is supposed to influence the counterion density via the Boltzmann factor:

$$n(r) = n(R) \exp \{ \beta e \Phi(r) \} \quad (2)$$

with the inverse temperature $\beta := 1/k_B T$ and k_B being Boltzmann's constant. Thus, the chosen normalization of the potential is $\Phi(R) = 0$.

In the following it is advantageous to change variables: The Bjerrum length $\ell_B := \beta e^2 / 4\pi\epsilon$ provides a convenient scale for quantifying electrostatic interactions (it is the distance, at which the Coulomb energy of two elementary charges equals $k_B T$), while the dimensionless Manning parameter $\xi := \lambda \ell_B / e$ measures the line charge density of the rod (it is equal to the number of elementary charges per Bjerrum length). We shall only be interested in the strongly charged case $\xi > 1$. Insertion of Eq. (1) into Eq. (2) results in the nonlinear PB equation which in terms of the reduced (dimensionless) electrostatic potential $y(r) := \beta e \Phi(r)$ and a screening constant $1/\kappa > 0$ with $\kappa^2 := 4\pi\ell_B n(R)$ reads

$$y'' + \frac{y'}{r} = \kappa^2 e^y \quad (3)$$

The appropriate boundary conditions for solving the PB equation are

$$y'(r_0) = -2\xi/r_0, \quad y'(R) = 0 \quad (4)$$

Eq. (3) has an analytical solution which can be written in the following way:

$$y(r) = -2 \ln \left\{ \frac{\kappa r}{\gamma \sqrt{2}} \cos \left(\gamma \ln \frac{r}{R_M} \right) \right\}. \quad (5)$$

The boundary conditions (4) yield two coupled, transcendental equations for the two integration constants γ and R_M :

$$\gamma \ln \frac{r_0}{R_M} = \arctan \frac{1-\xi}{\gamma} \quad (6)$$

$$\gamma \ln \frac{R}{R_M} = \arctan \frac{1}{\gamma} \quad (7)$$

Subtracting (6) from (7) eliminates R_M and provides an equation from which γ can be obtained *numerically*. The

second integration constant R_M , which we will refer to as the *Manning radius*, is then given by either of these equations. Note also that κ and γ are connected via $\kappa^2 R^2 = 2(1+\gamma^2)$, thus ensuring the chosen normalization of the potential.

The Manning radius R_M depends monotonically on ξ and for $\xi > 1$ one finds $R_M > r_0$. As discussed in the next section this is the regime in which counterion condensation occurs. If $\xi = 1$ then $R_M = r_0$, i.e., the Manning radius is located at the surface of the rod. A further decrease in ξ shifts R_M inside the cylinder and for $\xi = \ln(R/r_0)/(1 + \ln(R/r_0))$ both the Manning radius and γ vanish. Even smaller values of ξ render the integration constant γ complex. Still, the solution (5) can be extended by analytic continuation over \mathbb{C} .

Using Eqs. (2,5,6), the total charge per unit length, $Q(r)$, found within a cylinder of radius $r \in [r_0; R]$ can be determined by integration:

$$\begin{aligned} Q(r)/\lambda &:= 1 - \frac{1}{\lambda} \int_{r_0}^r d\bar{r} 2\pi\bar{r} e n(\bar{r}) \\ &= 1 - \left(1 - \frac{1}{\xi} \right) - \frac{\gamma}{\xi} \tan \left(\gamma \ln \frac{r}{R_M} \right) \end{aligned} \quad (8)$$

Since $n(r) > 0$, $Q(r)$ decreases monotonically from $Q(r_0) = \lambda$ to $Q(R) = 0$. The latter follows from Eq. (7) and is a consequence of global charge neutrality. It is instructive to use the quantity

$$P(r) := 1 - Q(r)/\lambda, \quad (9)$$

which is the *integrated probability distribution* of finding a mobile ion at distance r . In other words, it is the *fraction of counterions* found within a cylinder of radius r . In particular, at $r = R_M$ the last term in Q , as given in Eq. (8), vanishes, giving a fraction $1 - 1/\xi$ of ions within R_M . It can easily be verified that generalizing Eqs. (4, 6, 8) for counterions with valence v reduces to replacing $\xi \rightarrow \xi v$. Within PB-theory changing valence or electrostatic interaction strength affects the charge distribution function in the same way.

III. COUNTERION CONDENSATION: DEFINITION AND IDENTIFICATION

For $\xi > 1$ Eqs. (6) and (7) imply the inequalities

$$\frac{\pi}{\ln \frac{R}{r_0}} \geq \gamma \geq \frac{\pi}{\ln \frac{R}{r_0} + \frac{\xi}{\xi-1}}. \quad (10)$$

Since the two boundaries converge in the limit $R \rightarrow \infty$, they provide an asymptotic solution for γ and give rise to various limiting laws, which illuminate the behavior of the solution in the dilute limit. In particular, the reduced potential for $\xi > 1$ becomes¹⁴:

$$y(r) - y(r_0) = -2 \ln \frac{r}{r_0} - 2 \ln \left\{ 1 + (\xi - 1) \ln \frac{r}{r_0} \right\}, \quad (11)$$

which is up to a logarithmic correction identical to the potential of a rod with Manning parameter $\xi = 1$. This can be attributed to a condensation of counterions onto the

rod, which renormalize the line charge density. Indeed, the contact density $n(r_0)$ converges against the nonzero value

$$\lim_{R \rightarrow \infty} n(r_0) = \frac{\lambda}{\pi r_0^2 e} \frac{(\xi - 1)^2}{2\xi}, \quad (12)$$

suggesting the existence of a close layer which cannot be diluted away.

In order to establish an effective Manning parameter of 1, a fraction $f_\xi := 1 - 1/\xi$ of all counterions would have to condense onto the rod. In fact, f_ξ is a critical threshold in the following sense: For $0 < \alpha < 1$, $\xi > 1$ and the radius r_α defined as $r_\alpha := r_0 \exp\{\alpha/(\xi - 1)(1 - \alpha)\}$ one can show by using Eqs. (6–9) that

$$\lim_{R \rightarrow \infty} P(r_\alpha) = \alpha f_\xi. \quad (13)$$

Hence, in the limit of infinite dilution a fraction α (arbitrarily close to 1) of the fraction f_ξ stays within a *finite* radius r_α . It has thus been common practice to call f_ξ the *fraction of condensed counterions* or *Manning fraction*, although $\lim_{\alpha \uparrow 1} r_\alpha = \infty$. Actually, R_M diverges like \sqrt{R} , which follows directly from either of the asymptotic boundaries (10) for γ .

Investigating counterion condensation by means of computer simulations requires a criterion which identifies condensed ions. Here we show that the *functional form* of the counterion distribution function suggests a simple rule for recognizing the Manning layer.

If the function P is known, the condensed counterion fraction can be characterized in the following “geometric” way: Eq. (8) shows that P viewed as a function of $\ln(r)$ is merely a *shifted tangens-function* with its center of symmetry at $\{\ln(R_M); f_\xi\}$. Since $\tan''(0) = 0$, Manning radius and Manning fraction can be found by plotting P as a function of $\ln(r)$ and *localizing the point of inflection*.

This property of P , derived within the framework of PB-theory, can in turn be used to *define* the condensed fraction. It provides a suitable way to quantify counterion condensation beyond the scope of PB-theory, and it is exact in the PB-limit without added salt, by construction.

Our counterion condensation criterion can be reformulated in terms of the counterion density $n(r)$: If P has a point of inflection as a function of $\ln r$, $dP/d \ln(r)$ must have a stationary point there. Using Eqs. (8,9), it follows that $r^2 n(r)$ must have a stationary point (which in the simple salt free case is actually a minimum).

On this occasion we would like to briefly discuss three other methods which have been used to measure counterion condensation and point out their shortcomings. The notion of a condensed layer closely surrounding the rod suggests to determine the condensed fraction by simply counting the ions within a certain (small) distance of the rod, say, a few diameters or one screening length, $1/\kappa$ ¹⁵. This amounts to making a prior assumption about the Manning radius. Such a procedure is not only arbitrary; moreover, the PB Manning radius depends on the polyelectrolyte density and diverges like \sqrt{R} in the dilute limit. If this is not taken into account, the condensed

fraction is either underestimated (for fixed condensation distance) or overestimated (for a distance proportional to the screening length, $1/\kappa$ of the counterions, which is proportional to R).

Conversely, one could assume that the condensed fraction is *always* given by $1 - 1/\xi$ and thereby obtain the size of the condensed layer, e.g. when salt is added to the system.¹⁶ Although being exact in the salt free PB limit, this criterion excludes by definition the possibility that any effects beyond the *mean-field* level (like correlations) or the presence of salt also modify the *fraction* of condensed counterions. It also does not predict a crossover to a high salt regime where all counterions are condensed solely due to the presence of the salt (see Sec. VI).

Finally, one could be tempted to use the electrostatic binding energy to distinguish between uncondensed and condensed counterions – the latter having a binding energy to the rod of more than $k_B T$ ¹⁷. In other words, an ion at distance r is condensed if $y(r) > 1$. Within salt free PB theory this however is not a suitable criterion, since the electrostatic potential at the Manning radius, $\Phi(R_M)$, *diverges* in the limit $R \rightarrow \infty$, as can easily be derived using either of the asymptotic expressions in Eq. (10). Hence, the particular value $k_B T$ for the electrostatic energy is in no way special.

Let us thus repeat that the inflection point criterion employed in the present work has the advantages of (i) not already by definition fixing the amount of condensed counterions (f_ξ and R_M can be determined independently of each other), (ii) reproducing the salt free PB limit, namely $P(R_M) = 1 - 1/\xi$, and (iii) quantifying the break down of the coexistence of condensed and uncondensed counterions in the high salt limit, as will be shown in Sec. VI.

In concluding this section we want to bring the appearance of the logarithm in the inflection point criterion in relation to the fact that $\ln(r)$ is the *Green function* of the cylindrically symmetric Laplacian. In the corresponding spherical problem of charged colloids the Green function $1/r$ would be the appropriate choice for plotting the radial coordinate.¹²

IV. COMPARISON OF PB THEORY WITH SIMULATIONS: NO ADDED SALT

In this section we supplement the results of salt free PB theory with computer simulations of a cell-like model, with particular emphasis on the role of Manning parameter and valence. Details of the model, the simulations and our notation conventions are summarized in the Appendix.

Fig. 1 shows the counterion distribution functions, $P(r)$, for three systems with monovalent counterions, $l_B/r_0 = 1$, $R/r_0 = 123.8$ and $\xi \in \{0.96, 1.92, 2.88\}$, i.e., counterion condensation is expected to occur for the latter two. As suggested in the previous section the functions are plotted using a logarithmically divided r -axis. Note that in all our PB calculations and simulations the radius of the rod was $r_0 = \sigma$ where σ is the small ion diameter, used in the simulations (see Appendix).

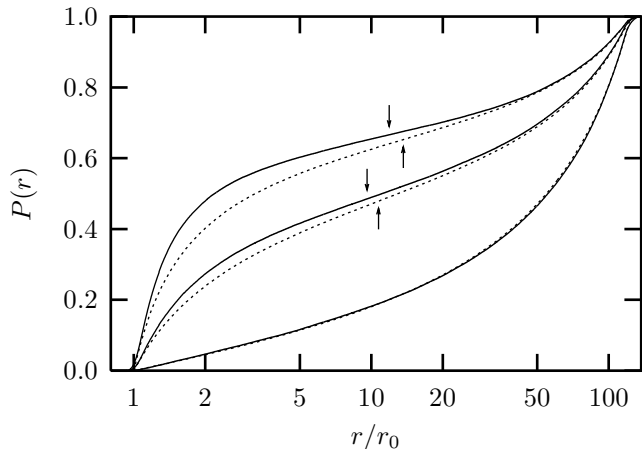


FIG. 1. Simulated counterion distributions (solid lines) and PB-results (dotted lines) for a monovalent system with $r_0 = 1\sigma$, $R/r_0 \approx 123.8$ and (from bottom to top) $\xi \in \{0.96, 1.92, 2.88\}$. The \uparrow -arrows mark the inflection points in the PB-distribution while the \downarrow -arrows mark those points in the measured distributions. Note the logarithmically divided r -axis in the present and the following figures.

R/r_0	2.06	3.87	7.74	15.5	31.0	62.0	124
$\xi = 1.92$	0.56	0.57	0.56	0.54	0.53	0.51	0.49
$\xi = 2.88$	0.78	0.76	0.73	0.70	0.69	0.67	0.67

TABLE I. Measured condensation fraction f_ξ for various monovalent systems with $r_0 = \sigma$, which differ in cell size R and thus polyelectrolyte density. Within PB theory $f_\xi = 1 - 1/\xi$, giving $f_{1.92} \approx 0.479$ and $f_{2.88} \approx 0.653$ – independently of R . Note that the counterion distribution functions for $R/r_0 = 124$ are shown in Fig. 1.

For the system with $\xi = 0.96$ in Fig. 1 the agreement between simulation and PB theory is excellent – deviations are almost within the linewidth of the plotted curves. For the other two cases the agreement fails quantitatively, but *not* qualitatively: The shape of the distribution function remains largely unchanged. The curves for $P(r)$ lie above the PB result for all r , indicating a stronger condensation than predicted by *mean-field* theory. Importantly, for $\xi > 1$ the simulated curves display a point of inflection. As described in the previous section this can be used to define a Manning radius and a condensation fraction, which permits to quantify *how much* the condensation is stronger. This is summarized for a range of densities in Table I, where it can be seen that deviations towards higher condensation are stronger for dense systems and relax towards the PB prediction upon dilution.

Note that in Fig. 1 the measured fraction f_ξ is *larger* than the PB-prediction, while the corresponding Manning radius is *smaller*. Since however within PB-theory R_M increases monotonically with ξ , the measured curves cannot be modelled by a PB distribution with a somewhat larger *effective* ξ .

As already mentioned, within PB theory the shape of the integrated distribution function, $P(r)$, depends on the Manning parameter ξ and the counterion valence v only via the product ξv . We show that this is a property seen on the *mean-field* level only. In addition to the PB

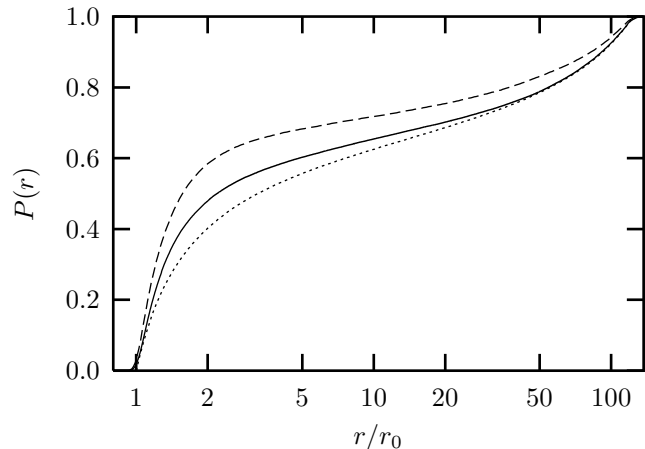


FIG. 2. Comparison of Manning parameter and valence. The simulated system from Fig. 1 with $\xi = 2.88$ (solid curve) and its PB-solution (dotted curve) are contrasted with a simulation where the Manning parameter is three times smaller but the counterions are trivalent (dashed curve).

result and the simulation of the system with $\xi = 2.88$ already shown in Fig. 1 the simulated $P(r)$ curve for a system with *trivalent* counterions and $\xi = 2.88/3 = 0.96$ is displayed in Fig. 2. The corresponding $P(r)$ indicates an even stronger condensation than the simulation for $\xi = 2.88$ and monovalent counterions.

There are two principle ways in which PB theory can fail: (i) the neglect of excluded volume interactions (“point-like” ions) and (ii) missing correlations. For the first point there is a simple self-consistency check: The counterion density is highest at the surface of the inner rod and e.g. in the limit $R \rightarrow \infty$ given by Eq. (12), but counterions with a finite size might not be able to give rise to a density as large as that. This consequently limits the range of applicability of the PB approximation towards not too large ions, not too small cylinders and not too strong electrostatics. In our simulations we are below that limit. Excluded volume interactions – if present – reduce the contact density and hence the counterion condensation; this however is not found in the simulations. The observed stronger condensation must therefore be attributed to correlations neglected in the PB approach. Since an increase in density goes along with an increase of correlations, this explanation seems to be intuitively correct and it is also supported by more involved theories, which go beyond the *mean-field* level.^{18,19}

V. COUNTERION CONDENSATION IN THE PRESENCE OF SALT

The central question to be discussed in this section is the following: Can the concept of counterion condensation be extended to the case of added salt?

Note first of all that the salt corresponds to a new degree of freedom which comes along with its own length scale, namely, a Debye length $\ell_D := (8\pi\ell_B v^2 n)^{-1/2}$, where v is the valence of the (for simplicity) symmetric salt and n is its density. It is of central importance how this new length relates to the characteristic length R_M of the condensation structure: If ℓ_D is large com-

pared to R_M , this structure is preserved; if ℓ_D is smaller, it dictates the shape of the charge distribution function and the condensation structure is no longer present.

Counterion condensation becomes apparent in the behavior of the charge distribution function for $R \rightarrow \infty$, hence one should also investigate this limit in the presence of salt. This however is crucially dependent on the chosen *ensemble*, i.e., whether the limit is performed at constant number N of salt molecules or at constant chemical potential μ .

In the constant N case ℓ_D is proportional to R and thus diverges faster than the Manning radius R_M , which only scales like \sqrt{R} . For sufficiently large R the condensation structure will therefore be visible and the condensation criterion will be the same as in the salt free case. Conversely, for sufficiently high density or number of salt molecules, ℓ_D will be *smaller* than the Manning radius, thus modifying the condensation structure. Since the latter is a new mechanism for compensating the rod charge, it is no longer sensible to use the concept of Manning condensation in this limit. It remains the task of clarifying the crossover from *counterion condensation* to *screening*, which is subject of the following section.

This line of reasoning needs a little modification if the added salt has a higher valence than the counterions, since then it will preferably be the salt ions which will condense onto the rod. Two cases have to be distinguished:

1. Already a fraction of the negative salt ions of highest valence could completely neutralize the rod. If these ions are taken to be the “true” counterions and all the rest (including the “original” counterions) is denoted as “salt”, one can expect a Manning limiting behavior typical for the highvalent new counterions.
2. There is not enough salt to completely neutralize the rod with the negative salt ions. This is just as complicated as the case of no salt but different species of counterions and will not be pursued further in this paper.

Quite differently, in the constant μ case the Debye length of the salt will remain *finite* in the limit $R \rightarrow \infty$ and consequently smaller than the diverging Manning radius. The condensation structure will always be wiped out in the dilution limit and it is not possible to produce a condensation criterion along the lines of the salt free case. We therefore prefer to work in the constant N ensemble.

VI. POISSON-BOLTZMANN EQUATION FOR CONSTANT NUMBER OF SALT MOLECULES

Assume that in addition to the monovalent counterions of the positively charged rod the cell contains K different $v : v$ salts of concentrations \bar{n}_v with $v = 1 \dots K$. The overall concentration of negative monovalent ions is thus $\bar{n}_1 + m$ with $m = \lambda/e\pi R^2$ where m is the contribution due to the counterions of the rod.

The free energy $F = U - TS$ accounts for the internal electrostatic energy, U , and the translational entropy, S ,

of the mobile ions in solution. It can be written in terms of the electrostatic potential, Φ , and the local ion concentrations n_v and n_{-v} of positive and negative ions of valence v , respectively. Within *mean-field* theory, F is given by

$$F = \int_V d^3r \left[\frac{\epsilon}{2} (\nabla\Phi)^2 + k_B T \sum_{\substack{v=-K \\ v \neq 0}}^K n_v \ln \frac{n_v}{\bar{n}_v} \right] \quad (14)$$

where $\bar{n}_{-v} = \bar{n}_v$ (for $v = 2 \dots K$) and $\bar{n}_{-1} = \bar{n}_1 + m$ denote the concentrations of the negatively charged mobile ions.

As discussed in the above section, we are interested in the constant N ensemble, i.e., the case that for each ionic species the number of ions within the cell of volume V is conserved. The local equilibrium concentrations, n_v , have thus to be derived under the constraints

$$\langle n_v \rangle \equiv \frac{1}{V} \int_V d^3r n_v = \bar{n}_v \quad (15)$$

The usual variation of F results then in the Boltzmann distributions for the local concentrations

$$n_v = \bar{n}_v e^{-vy - \mu_v} \quad (16)$$

where the chemical potentials $\mu_v = \ln(e^{-vy})$ ensure particle conservation.

Again we consider the rod sufficiently long allowing us to neglect end effects. Then, the electrostatic potential Φ and the local ion concentrations n_v depend only on the radial distance r to the rod midaxis.

Insertion of the local concentrations n_v into the cylindrically symmetric Poisson equation $\epsilon(\Phi'' + \Phi'/r) = -\sum_v v n_v$ leads to the Poisson-Boltzmann equation

$$y'' + \frac{y'}{r} = -4\pi\ell_B \sum_{v=-K}^K v \bar{n}_v \frac{e^{-vy}}{\langle e^{-vy} \rangle} \quad (17)$$

This equation has to be solved subject to the boundary conditions (4), i.e. the same as for the salt free case.

Numerical solutions of Eq. (17) can be found employing a Newton-Raphson iteration scheme in which the chemical potentials $\mu_v = \ln(e^{-vy})$ are updated after each iteration step. Once a solution $y(r)$ is found, the *integrated charge distribution function* of the mobile ions

$$P(r) = \frac{e}{\lambda} \int_{r_0}^r dr' 2\pi r' \sum_{v=-K}^K v n_v(r') \quad (18)$$

can simply be calculated by $P(r) = 1 + ry'(r)/2\xi$ which follows from inserting the Poisson equation into Eq. (18) and carrying out the integration under consideration of the boundary conditions (4). Since $P(r)$ is a measure of the fraction of the overall electrolyte charge found within a cylinder of radius r , we must have $P(r_0) = 0$ and $P(R) = 1$. Note that Eq. (18) is a natural generalization of the distribution function from Eq. (9), but its interpretation as an integrated probability distribution (or fraction of counterions) is only valid in the salt free case.

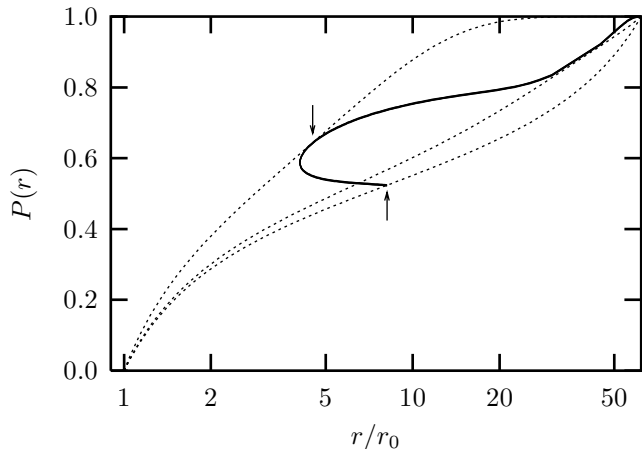


FIG. 3. PB results (dotted curves) for the integrated charge distribution function $P(r)$ for a system characterized by $r_0 = \sigma$, $R/r_0 = 61.9$, $\xi = 2.1$, $\lambda = 0.96 e/r_0$, monovalent counterions and different numbers of 1 : 1 salt molecules per rod segment of length $L = 250 r_0$: from bottom to top $N \in \{0, 104, 3070\}$. Note that the number of counterions corresponding to L is $M = 240$. The thick solid curve shows the locus of inflection points, i.e., the union of all inflection points of the functions $P(r)$. The \uparrow -arrow marks the location of the salt free Manning inflection point and the \downarrow -arrow shows where it annihilates with one of the new salt inflection points. The branch of the locus between these two arrows indicates the range in which the concept of Manning condensation is meaningful.

To investigate the condensation criterion in the presence of monovalent salt we have calculated the *mean-field* potential, $y(r)$, solving the PB equation for a system characterized by $r_0 = \sigma$, $R/r_0 = 61.9$, $\lambda/e = 0.96/r_0$, $\xi = 2.1$ and a variable number of salt molecules. To facilitate the comparison with computer simulations in the next section let us express the number of monovalent salt molecules, N , with respect to a rod segment of length $L = 250 r_0$. The corresponding cell volume that contains the mobile ions is then $V = L\pi R^2$ and the Debye length is $\ell_D = (8\pi\ell_B N/V)^{-1/2}$. Note that the line charge density $\lambda = 0.96 e/r_0$ implies a number $M = 240$ positive charges found on the rod segment of length $L = 250 r_0$.

From the numerical solutions of $y(r)$ we have determined all inflection points of $P(r)$ plotted against $\ln r$. These inflection points are solutions of the equation $d^2 P(r)/d(\ln r)^2 = 0$. In Fig. 3 we present the inflections points (dotted line) starting from $N = 0$ up to $N = 3070$. For larger values of N no further inflection points are found. We also show the integrated charge distributions (solid lines) for $N = 0, 104$ and 3070 , corresponding to Debye lengths of $\ell_D/r_0 = \infty, 22.9$ and 4.2 , respectively.

The location of the inflection point for $N = 0$ coincides with R_M , thus indicating a fraction of condensed counterions of $P(R_M) = 1 - 1/\xi$. Increasing N by adding salt shifts the inflection point to smaller values of r . That is, the layer of condensed counterions contracts, which is in accord with other condensation criteria mentioned in Sec. III. Importantly, the *amount* of condensed counterions is only marginally increased in the presence of monovalent salt. From a certain N on (in Fig. 3 we find

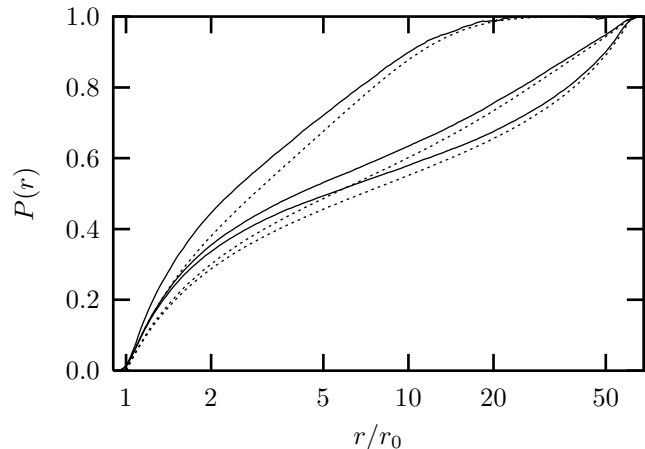


FIG. 4. Simulated curves $P(r)$ for the three systems from Fig. 3 (solid lines) and the corresponding PB results (dotted curves).

$N = 104$) two more inflection points appear in the high r/r_0 region. This happens typically for a corresponding Debye length being of the order of the cell size itself, indicating the appearance of a characteristic, salt induced, change in the convexity of P (as a function of $\ln r$).

Upon a further increase in N one of the two new inflection points shifts towards smaller r/r_0 values, finally fusing with the Manning inflection point and “annihilating” with it. Roughly speaking, we find the inflection points to vanish if the Debye length characterizing the salt content becomes smaller than the radius of the condensed layer. This suggests a break-down of the need to distinguish between condensed and uncondensed counterions once the typical salt screening length interferes with the size of the condensed counterion layer. Indeed, for a very high salt content, where the Debye length is much smaller than the radius of the rod, the solution of the PB equation would be the one of a charged plane and one may consider all excess counterions being condensed no matter what the charge density of the rod is.

VII. COMPARISON OF PB THEORY WITH SIMULATIONS: ADDED SALT

In this section we again compare the numerical results of the PB equation – this time in the presence of salt – with computer simulations. We reinvestigate the systems in Fig. 3 with $\xi = 2.1$, monovalent counterions and number of salt molecules $N = 0, 104$, and 3070 with respect to a rod segment of length $L = 250 r_0$. The results of the computer simulations and the corresponding *mean-field* calculations are presented in Fig. 4. Like in the salt free case the computer simulations show a more pronounced condensation effect towards the rod, which we again attribute to ion-ion correlation effects. Still, the shape of the distribution functions remains qualitatively the same. Note in particular that the appearance and disappearance of two points of inflection at $N = 104$ and $N = 3070$ respectively, which leads to extremely small curvatures in the PB distribution functions, also leads to very straight regions in the *measured* distribution functions. The crossover from Manning condensation to

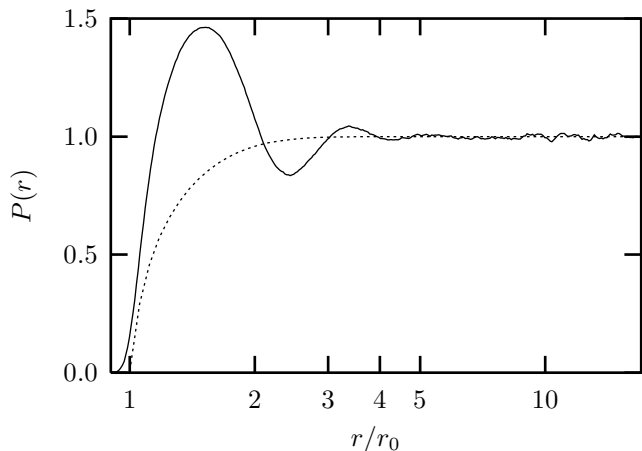


FIG. 5. The integrated charge distribution function, $P(r)$, for a system characterized by $r_0 = \sigma$, $R/r_0 = 15.5$, $\xi = 4$, $\lambda/e = 0.96/r_0$, $N = 1000$ molecules of a divalent salt and $M = 60$ monovalent counterions corresponding to a rod segment of length $L = 62.5r_0$. The simulation (solid curve) shows a pronounced overcharging-effect, in contrast to PB-theory (dotted curve).

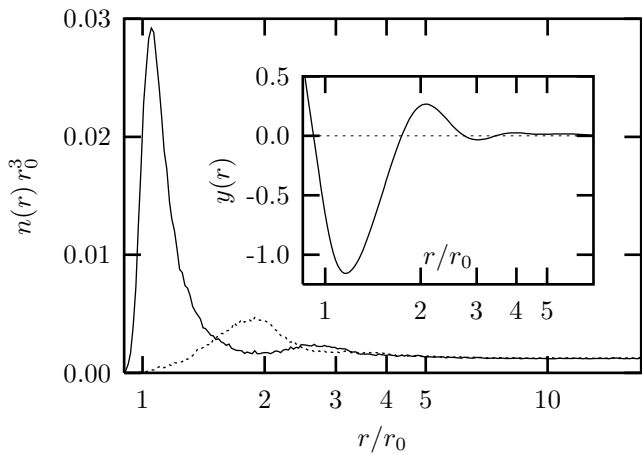


FIG. 6. The densities $n_{-2}(r)$ (solid line) and $n_{+2}(r)$ (dotted line) of negative and positive salt ions, respectively, for the same system presented in Fig. 5. The inlay shows the electrostatic potential $y(r)$.

screening, as described within PB theory, can thus be expected to be essentially correct.

The PB approach fails to describe the physical situation if one or more of the following points apply: (i) the electrostatic interactions are strong, (ii) the counterions are multivalent and (iii) the density is high. A simulation under such conditions can be inspected in Fig. 5. In this system we have $r_0 = \sigma$, $R/r_0 \approx 15.5$, $\xi = 4$, 60 monovalent counterions, and 1000 molecules of a 2:2 salt (giving a Debye length of roughly $0.33 r_0$, i.e., smaller than the ion diameter). Here $P(r)$ overshoots unity, showing a charge reversal of the rod at distances around $r \approx 1.5 r_0$, while the simple PB prediction is clearly *qualitatively* off. This phenomenon is usually referred to as *overcharging* and has been predicted for the primitive cell model from HNC¹⁹ or modified Poisson-Boltzmann¹⁸ calculations.

Since $P(R) = 1$, the overshooting above 1 at small distances implies the existence of a range of r -values at which the system is locally *positively* charged (i.e., with

the same charge as the rod), such that $P(r)$ can eventually decay to 1. This is seen in Fig. 6, which shows that $n_{+2}(r) > n_{-2}(r)$ at $r \approx 2 r_0$. Since $P(1.5) \approx 1.45$, the rod and its innermost layer of condensed ions could be viewed as an effective rod of radius $1.5 r_0$ which is negatively charged with Manning parameter $\xi = 1.8$. Since this value is again larger than 1, it entails ion condensation (this time of the positive ions). In fact, it even leads to a second overcharging, as can clearly be seen in Fig. 5, where $P(r)$ – in decaying from 1.45 – overshoots the value of 1 again. Overcharging can thus give rise to layering; in the presented example no less than three layers can clearly be made out. These local charge oscillations also reflect themselves in oscillations of the electrostatic potential, as demonstrated in the inset of Fig. 6. Note that these oscillating potentials will also have pronounced effects on the interaction *between* such rigid polyelectrolytes.

CONCLUSIONS

We have revisited counterion condensation with and without added salt for a solution of rigid polyelectrolytes within the cell model approximation. It was recapitulated that on the level of PB theory with no added salt a simple geometric method locates the condensation radius R_M as well as the fraction of condensed counterions. This geometric method consists in finding the inflection point of the integrated probability distribution P plotted as a function of $\ln r$. Without added salt, the locations of the inflection point as well as the Manning radius R_M , where a fraction of $1 - 1/\xi$ counterions are condensed, are identical.

A key point in the present work was to extend the inflection point based counterion condensation criterion to the case of added salt and to compare its implications as predicted by PB theory and by computer simulations. Our motivation for introducing this new condensation criterion was (i) not already by definition to fix the amount of condensed counterions, (ii) to reproduce the salt free PB limit, namely $P(R_M) = 1 - 1/\xi$, and (iii) to predict a counterion condensation break down in the high salt limit. We are not aware of any other condensation criterion that fulfills all these requirements at the same time.

Upon addition of monovalent salt we found PB theory to predict counterion condensation within a somewhat smaller region around the charged rod. This is in accord with other studies^{20,21} using different condensation criteria^{16,17,22}. Importantly, the fraction of condensed counterions did not exhibit a strong salt dependence thus supporting a principal idea in Manning condensation: The number of condensed counterions does not depend on salt. Yet, this observation must break down in the high salt limit, where the screening length of the salt is on the order of the size of the condensed counterion layer. Indeed, our new condensation criterion naturally predicts this to happen.

All these behaviors were well reproduced by our computer simulations. In fact, the agreement between simulation and the corresponding *mean-field* level calculation

is remarkably good for systems with a Manning parameter $\xi < 1$. Upon increasing the counterion density, valence, or the Manning parameter, the simulations predict consistently a somewhat stronger condensation. We have argued that this finding is due to ionic correlations not present in PB theory. To test this assumption, we have also performed a simulation of a system in a highly concentrated divalent salt environment. Here we clearly saw the phenomenon of overcharging, which a corresponding PB calculation was unable to reproduce.

We note finally that our MD simulations suggest the usability of the counterion condensation criterion beyond the PB cell model approximation. In fact, we have observed inflection points in the integrated probability distribution functions in systems very distinct from the rigid rods employed in the present study, namely for flexible polyelectrolytes in the presence of multivalent counterions and for flexible polyelectrolytes in poor solvents with monovalent counterions²³.

ACKNOWLEDGMENTS

CH and MD thank G. Manning for useful conversations and for bringing Belloni's work to our attention. This work has been started at the ITP, Santa Barbara, whose financial support under NFS grant No. PHY-94-07194 is gratefully acknowledged. SM wishes to thank SFB 197 for its support.

APPENDIX: DETAILS OF THE SIMULATION

The system used to study counterion condensation consists of a cubic simulation box of length L_b , a charged rod along the main diagonal, the appropriate amount of counterions necessary for electric neutrality and possibly some additional salt. Upon switching on 3d-periodic boundary conditions a triangular array of infinitely long charged rods is modelled. Note that in PB theory we approximate the corresponding Wigner-Seitz-cell by a cylindrically symmetric unit cell of the same volume (implying $R = L_b/\sqrt{\pi\sqrt{3}}$) thus rendering the PB equation one-dimensional.

Apart from electrostatic interactions all ions are subject to a purely repulsive Lennard-Jones potential, giving an excluded volume and a corresponding ion-diameter σ . Further, the rod is modelled as an immobile string of such spheres, having the separation 1.042σ . The distance of closest approach to the cylinder, i.e. r_0 , turns out to be essentially 1σ .

The electrostatic interactions in this periodic boundary geometry have been computed with the help of P³M routines²⁴ and a Langevin thermostat²⁵ has been implemented to drive the system into the canonical state. A more detailed description of our simulation method will be presented in a forthcoming publication²⁶.

- ¹ see Refs. in G. S. Manning, Ber. Bunsenges. Phys. Chem **100**, 909 (1996).
- ² G. S. Manning, J. Chem. Phys., **51**, 924, 934, 3249 (1969).
- ³ F. Oosawa, *Polyelectrolytes*, Marcel Decker, New York, 1970.
- ⁴ D. Stigter, Prog. Colloid Polym. Sci. **65**, 45 (1978); D. Stigter, Biophys. Journal, **69**, 380 (1995).
- ⁵ S. Lifson, and A. Katchalsky, J. Polym. Sci. **13**, 43 (1953).
- ⁶ A. Katchalsky, Pure Appl. Chem., **26**, 327 (1971).
- ⁷ T. Alfrey, P. Berg, and H. J. Morawetz, J. Polym. Sci. **7**, 543 (1951).
- ⁸ R. M. Fuoss, A. Katchalsky, S. Lifson, Proc. Natl. Acad. Sci. USA **37**, 579 (1951).
- ⁹ B. H. Zimm, and M. Le Bret, J. Biomol. Struct. Dyn. **1**, 461 (1983).
- ¹⁰ M. Le Bret and B. H. Zimm, Biopol. **23** 287 (1984).
- ¹¹ G. Manning, Journal of Biomolecular Structure and Dynamics, **16**, 461, (1998); G. Manning, private communication.
- ¹² L. Belloni, M. Drifford, and P. Turq, Chem. Phys. **83** 147 (1984); L. Belloni, Colloids and Surfaces **A 140**, 227 (1998).
- ¹³ Within Poisson-Boltzmann theory the dielectric constant of the cylinder is irrelevant for symmetry reasons. See, however, J. Skolnick and M. Fixman, Macromolecules **11**, 867 (1978).
- ¹⁴ For an alternative, explicit derivation see Appendix A in: R. R. Netz and J.-F. Joanny, Macromolecules **31**, 5123 (1998).
- ¹⁵ M. Mandel, J. Phys. Chem. **96** 3934 (1992).
- ¹⁶ M. Gueron and G. Weisbuch, Biopol. **19** 353 (1980).
- ¹⁷ G. Lamm, L. Wong and G. R. Pack, Biopol. **34** 227 (1994).
- ¹⁸ T. Das, D. Bratko, L. B. Bhuiyan and C. W. Outhwaite, J. Phys. Chem. **99**, 410 (1995). T. Das, D. Bratko, L. B. Bhuiyan and C. W. Outhwaite, J. Chem. Phys. **107**, 9197 (1997).
- ¹⁹ E. Gonzales-Tovar, M. Lozada-Cassou, D. Henderson, J. Chem. Phys. **83**, 361 (1985).
- ²⁰ P. Mills, C. F. Anderson, M. T. Record Jr., J. Phys. Chem. **89**, 3984 (1985).
- ²¹ C. S. Murthy, R. J. Bacquet, P. J. Rossky, J. Phys. Chem. **89**, 701 (1985).
- ²² E. Rajasekaran and B. Jayaram, Biopol. **34** 443 (1994).
- ²³ M. Deserno, C. Holm, U. Micka, K. Kremer, work in progress.
- ²⁴ R. W. Hockney and J. W. Eastwood, *Computer Simulation Using Particles*, IOP 1988. M. Deserno and C. Holm, J. Chem. Phys. **109** 7678 (1998); *ibid.* 7694.
- ²⁵ G. S. Grest and K. Kremer, Phys. Rev. **A33**, 3628 (1986).
- ²⁶ M. Deserno, C. Holm, in preparation.